Matching of Dental X-rays for Human Forensic Identification

by

Maja Omanovic

A thesis
presented to the University of Waterloo
in fulfilment of the
thesis requirement for the degree of
Master of Mathematics
in
Computer Science

Waterloo, Ontario, Canada, 2006

I hereby declare that I am the sole author of this thesis. This is a true copy of the thesis, including any required final revisions, as accepted by my examiners.

I understand that my thesis may be made electronically available to the public.

Abstract

Dental records have been widely used as tools in forensic identification. With the vast volume of cases that need to be investigated by forensic odontologists, a move towards a computer-aided dental identification system is necessary. We propose a computer-aided framework for efficient matching of dental x-rays for human identification purposes. Given a dental x-ray with a marked region of interest (ROI), we search the database of x-rays (presumed to be taken from known individuals) to retrieve a closest match. In this work we use a slightly extended Weighted Sum of Squared Differences (SSD) cost function to express the degree of similarity/overlap between two dental radiographs. Unlike other iterative Least Squares methods that use local information for gradient-based optimization, our method finds the globally optimal translation. In 90% of the identification trials, our method ranked the correct match in the top 10% using a database of 571 images. Experiments indicate that matching dental records using the extended SSD cost function is a viable method for human dental identification.

Acknowledgments

I would like to extend my deepest gratitude to my supervisor, Professor Jeff Orchard, for his expert guidance and mentorship. This work would not have been possible without his encouragement, support and friendship. I would also like to thank Professors Covvey and Wan for taking time out of their busy schedules to be a part of my thesis committee.

Dr. Sweet of BOLD lab and Dr. Barlow of University of Toronto offered much-appreciated advice and thought-provoking ideas at the beginning of my research. I am thankful to Dr. Lam of University of Toronto for providing the radiographs used in the experiments.

My sincere thanks to Professor Ioana Coman, who has inspired me to continue my studies in the field of Computer Science. Her friendship and advice have been invaluable.

I would like to extend my appreciation to my colleagues in the Scientific Computation Group for providing a productive environment to work in. Special thanks to my friends Alexei Ramotar, Igor Bogdanovic, Dragan Mirkovic, Sinisa Bjelica, Jessica Socha and Omar Halabieh, for making my stay in Waterloo fun and enjoyable. Thank you for all the great memories. My sincere appreciation is extended to Goran Bjedov for his genuine care, encouragement and support. I will always treasure your positive influence on my life. I would also like to thank the Bogdanovic family for giving me a home away from home. Their love and care are greatly appreciated.

Finally, I am greatly indebted to my family for their continued love and support. Thank you to my mother Dara and my brother Miran for always being there for me. Without your love and support none of this would have been possible. Thank you to my boyfriend David Browne for taking care of me and providing moral support throughout my thesis work. Your companionship, love and encouragement have been precious.

Dedication

For my mother Darinka, my brother Miran and my late father Zlatko, whose love nourishes my soul.

Contents

List of Tables

List of Figures

Chapter 1

Introduction

July 17, 2006, a tsunami south of Java Island reportedly killed 600 people, leaving 150 still missing. August 28, 2005, hurricane Katrina was upgraded to a Category 5 storm. It was one of the five deadliest tropical storms in the United States claiming 1,836 lives. December 26, 2004, the Indian Ocean Tsunami killed an estimated 275,000 people with thousands still missing. August 17, 1999, an earthquake of magnitude 7.4 on the Richter scale lasted 45 seconds and claimed over 17,000 lives in northwestern Turkey. September 1, 2004, a terrorist attack on a Beslan school in Russia killed 344 civilians, of which 186 were children. March 11, 2004 a coordinated bombing of commuter trains in Madrid, Spain killed 191 people. September 11, 2001, terrorists crashed commercial airliners into the World Trade Center and Pentagon killing 2,976 people.

Natural and man-made disasters of catastrophic magnitudes are unfortunately not unfamiliar to any of us. As a result of these terrorist attacks and naturally-occurring phenomena, cities around the world incurred substantial structural, financial and human losses. Bombings, hurricanes, earthquakes and tsunamis ravaged our communities leaving behind complete devastation, dust, ruins and nameless bodies. Regrettably, relief and recovery efforts too often require assistance from the forensic identification task force. These forensic specialists attend at the disaster sites with the primary objective of identifying the victims as soon as possible.

Early identification is mostly done by fingerprinting and DNA analysis methods. However, due to the severe weather conditions bodies are exposed to, fingerprints are often unavailable and the DNA is simply too hard to collect. In those cases, forensic scientists rely on teeth to establish the deceased individual's identity.

Unfortunately, mass disasters are not the only occasion during which human forensic identification based on dental remains is necessary. The following depicts another scenario: a person walking on a path through the forest comes across human skeletal remains. The deceased individual has been exposed to the elements to a point where no DNA is available. The teeth and bones hold the secret to the individual's identity. While it may sound like a scene from a TV show, it is not a far cry from reality. Often, bodies of an unidentified individual has decomposed to a point where best available information pertaining to the individual's identity are his/her teeth.So it is not uncommon for dental records to be used by law enforcement agencies in the process of human identification.

1.1 Human Forensic Identification

Forensic identification is a scientific profession focused on documenting, collecting and analyzing criminal evidence to identify specific objects from the traces they leave behind [1]. Human forensic identification ascertains the identity of a person based on specific physical and other measurable characteristics unique to each individual. It can be carried out prior to death, commonly referred to as antemortem (AM) identification, or after death, referred to as postmortem (PM) identification.

Individuals can be identified by fingerprints, earprints, handprints, retinal and iris scanning, voiceprinting, DNA fingerprinting, bones, teeth and many other features. These unique features specific to each individual, are called biometric identifiers. Biometric identifiers have been widely used by law enforcement agencies as tools in forensic identification. Bones and teeth are considered to be excellent biometric identifiers due to their ability to survive extreme conditions [2, 3]. Additionally, they are unaffected by early tissue decay that destroys most other

biometrics.

Although physiological characteristics (e.g. fingerprints and DNA) can produce an excellent match and significantly aid in the process of forensic identification, these identifiers are not always suitable or appropriate for postmortem identification. Temporal degradation is common for cases in which the identification is attempted more than a couple of weeks after death. Furthermore, severe circumstances encountered in mass disaster situations (earthquakes, floods, plane crashes etc.) tend to expedite tissue degradation leaving behind teeth as the key to unlocking the door to establishing positive identity.

1.1.1 Forensic Odontology

Forensic odontology is the branch of forensic science that is concerned with identifying human individuals based on their dental features [4]. Forensic odontologists attempt to establish the identity of an individual based on her/his dental records, which are usually kept as radiographic (x-ray) images. Both antemortem (AM) radiographs, dental x-rays obtained prior to death, and postmortem (PM) radiographs, dental x-rays obtained after death, are used in the process of matching. In order to identify an individual, there must be a presumptive identity for the deceased, so that PM dental records can be compared against specific AM records [5]. Accurate dental forensic identification entails a point-by-point comparison of a complete set of dental x-rays where"all points of comparison must match exactly, or in which differences can be explainable" [6].

According to a Federal Bureau of Investigation (FBI) report, as of December 31, 2005, there were 1,383 active unidentified person records in the National Crime Information Center (NCIC) database [7]. Along with that, there were 109,531 active missing person records. "It is estimated that at any point in time there are over 100,000 unsolved (missing and unidentified person (MUP) cases) in the National Crime Information Center, 60% of which have remained unsolved for 90 days or longer. Technically speaking, this large number of unsolved cases hinders the capabilities of search techniques currently employed" [8].

With the vast volume of cases that need to be investigated by forensic odontologists, a shift towards a computer aided dental identification system is inevitable. Automating the process of PM forensic identification will speed up the process of human identification and consequently save money. It will also provide emotional and psychological benefits to the families of missing persons who will be able to know the disposition of their family member without having to wait extended periods of time.

1.2 Current State of The Art

1.2.1 National Crime Information Center - United States

The National Crime Information Center (NCIC) maintains the only nationwide database containing dental records for both the missing and unidentified individuals. Before the individual's record is entered into the database, a forensic odontologist or a dental expert examines the dental x-rays and charts the morphological features for each individual tooth [9, 10]. Features and properties of the teeth such as dental work, pathology and dental restorations, presence/absence of a tooth, presence/absence of restorations, crown and root morphology, as well as periodontal tissue and other anatomic features are all closely examined and recorded. Dental charts are recorded according to the NCIC Dental Code Manual. An example of the Code Manual is shown in Fig. 1.1.

Once the dental features have been recorded, the dental chart is entered into the system along with the physical descriptors such as sex, age, height, weight, etc. Law enforcement personnel are then able to search the missing and the unidentified persons' database in an effort to establish the identity of the deceased individual. The process of comparing AM and PM records is carried out manually and both dental charts and physical descriptors are considered (with the emphasis on the latter). The NCIC computer searches the NCIC's MUP databases calculating the similarity score for each AM record. The score depends on the number of similar characteristics the AM record shares with the PM record. A record whose similarity

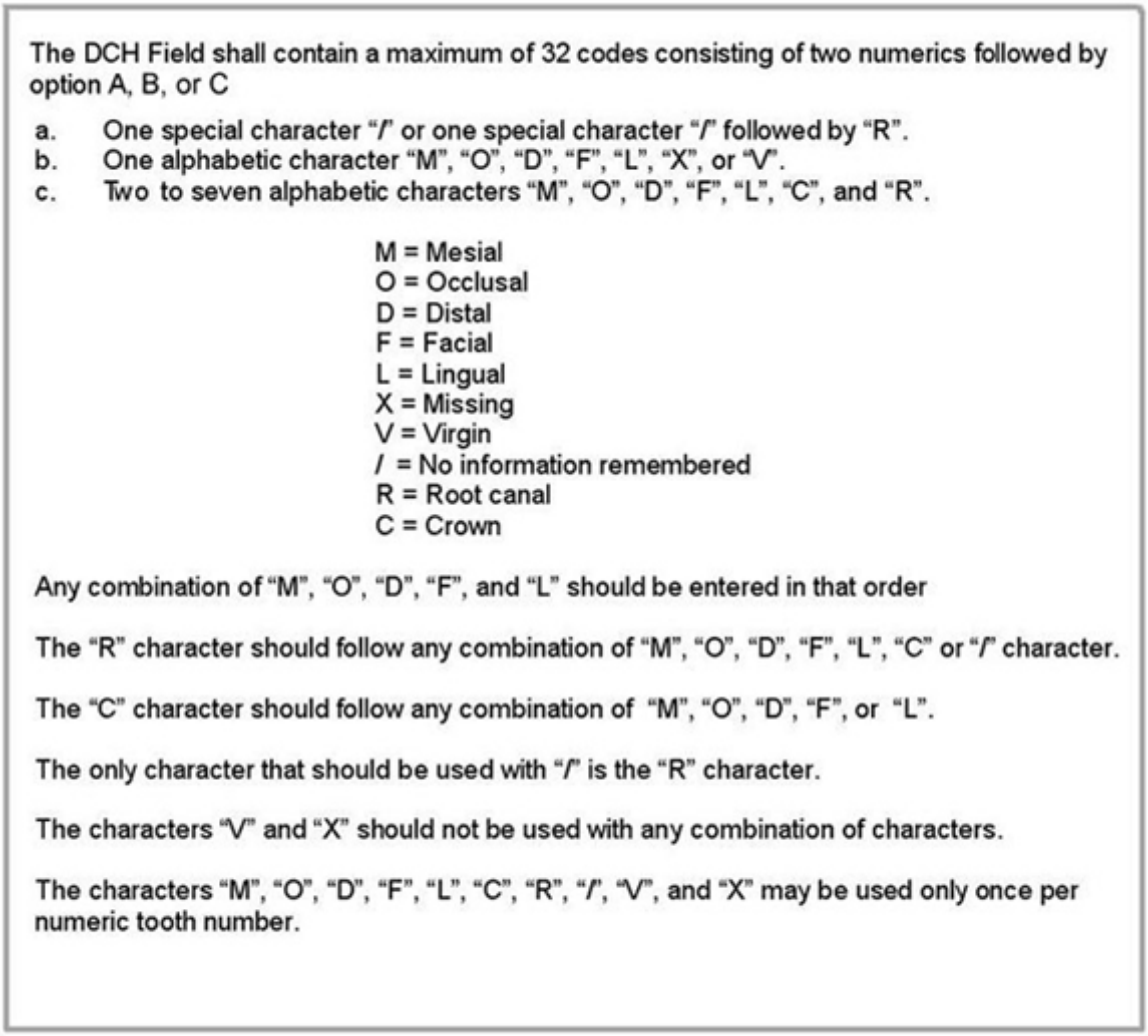

Figure 1.1: NCIC dental codes description and usage explanation

score is above a chosen threshold is identified as a possible match. Depending on the similarity between the AM and PM record, as well as their corresponding radiographs, the forensic expert rejects or confirms the candidate identity.

There are several problems with the NCIC system. Often, reports are collected by dentists or even personnel who are not necessarily trained in the field of forensic dentistry who produce inaccurate, biased and flawed dental charts. Additionally, NCIC Dental Code Manual forms tend to be complicated and subjective, leading to additional errors. As Kamb [11] points out, the method of similarity scoring itself is problematic. The similarity score is weighted heavily towards physical descriptors, but characteristics such as age, height and weight are often only estimates if the body was found in an advanced state of decomposition. Consequently, inaccurate results are obtained. The NCIC computer proved to be highly unreliable and prone to failure [11].

1.2.2 WinID and CAPMI

While NCIC's database maintains nationwide MUP records, Maryland, California and Washington maintain their own statewide MUP database. California and Washington use a Microsoft DOS-based Computer-Aided Postmortem Identification system (CAPMI), while Maryland uses a Windows-based program (WinID). Both of these systems exhibit better search capabilities than the FBI's NCIC dental search program [11].

Computer-Assisted Postmortem Identification System

The Computer-Assisted Postmortem Identification System was developed by the U.S. Army Institute of Dental Research to facilitate the process of human forensic dental identification. It is the first computer system of its kind. Although CAPMI lists best possible matches, final positive identification is still carried out by a forensic odontologist.

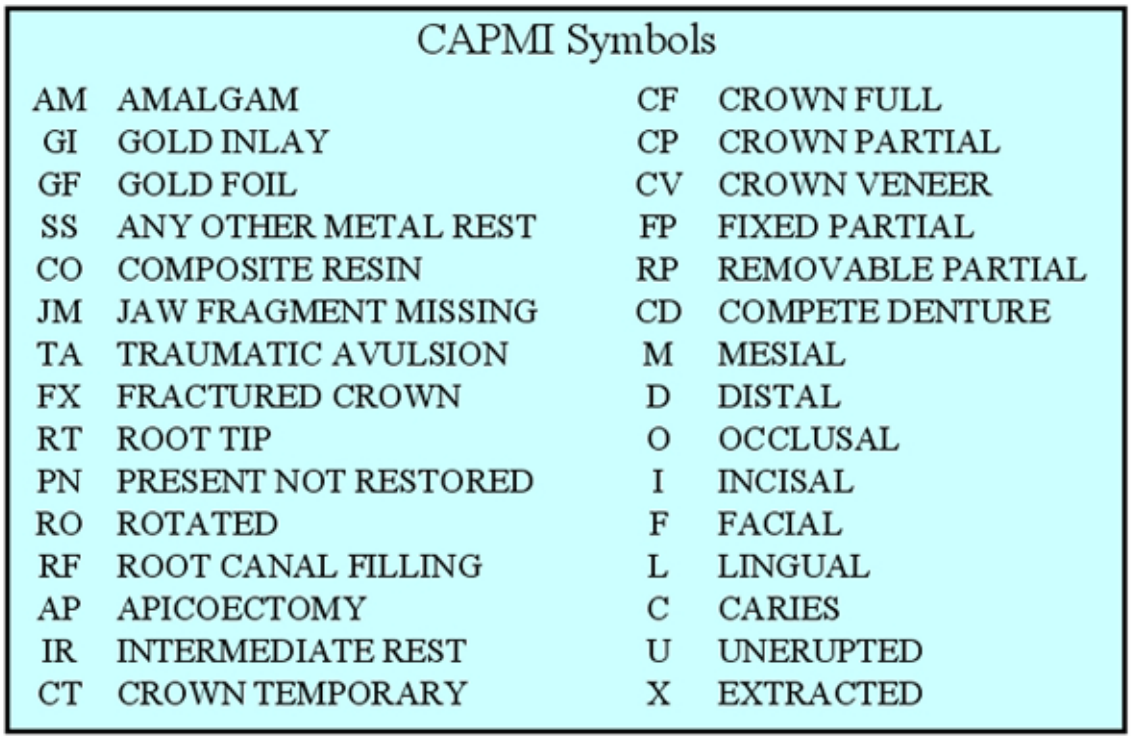

Figure 1.2: CAPMI dental codes

Similarly to the NCIC's dental search program, CAPMI uses both physical and dental descriptors in the process of human identification. Dental features are captured via predefined dental codes. The list of CAPMI codes is shown in Fig. 1.2. As a quality assurance measure, two individuals are responsible for charting the morphological features. Both the AM and PM charting involve an examiner and a recorder. After an examiner makes a statement of findings, it is visually confirmed and noted by the recorder. This redundancy aims at minimizing input errors. Dental features considered by the observers are: missing teeth, restorations, prosthetics, unique anatomy and presence/absence of pathology. Additionally, either exact physical descriptors (for AM charting) such as age, height, weight, gender, age and race, or their estimates (for PM charting) are recorded. Both PM and AM charting are accomplished using the CAPMI codes on AF Forms 1801 and

1802 respectively. Once the records are completed and entered into the database, the computer processes the information and compares ante/post mortem records searching for possible matches. A record is listed as a possible match if a significant level of similarity between the AM/PM pair is found.

WinID

WinID is dental software created by James McGivney, DMD, and it is offered as freeware. It is intended to assist forensic odontologists in establishing and maintaining a missing persons/unidentified bodies database [12]. WinID ranks potential matches between unidentified bodies and missing persons through the use of both dental and physical descriptors. Information regarding dental work, as well as physical descriptors describing an individual, are stored in the Microsoft Access Database. WinID uses MS Access's sorting and filtering capability for matching records. Similarly to NCIC's dental search program and CAPMI, WinID records dental features using a predefined set of dental codes. WinID dental codes, shown in Fig. 1.3 are an extension of CAPMI codes. An example of the dental chart entry in an individual's record is shown in Fig. 1.4.

WinID supports BMP as well as GIF and JPEG formats allowing inclusion of dental x-rays along with written information within an individual's record. WinID comes in 6 different supported languages, and easy switching between languages enables an extensive user group. This program is mostly used by forensic dentists, forensic odontologists, pathologists, coroners, medical examiners, forensic anthropologists and those in the law enforcement and criminal justice systems. However, as Dr. McGivney points out "the computer software does not make an identification, but it points the dentists in the right direction" [13].

Limitations

A major limitation of WinID and CAPMI dental matching systems is that they only capture artificial dental work. Characteristics inherent to teeth, such as crown and

Primary Codes

- **M – mesial** surface of tooth is restored.
- **O – occlusal** surface of posterior tooth is restored.
- **D – distal** surface of tooth is restored.
- **F – facial** surface of tooth is restored.
- **L – lingual** surface of tooth is restrored.
- **I – incisal** edge of anterior tooth is restored.
- **U** – tooth is **unerupted.**
- **V** – non-restored tooth - **virgin.**
- **X** – tooth is missing - **extracted.**
- **J** – tooth is **missing postmortem** or the clinical crown of the tooth is not present for examination. Also used for avulsed tooth. The root or an open socket is present, but no other information is present, but no other information is available.
- **/ - no information** about tooth is available.

Secondary Codes

- **A** – an **anomaly** is associated with this tooth. Specifics of the anomaly may be detailed in the comments section.
- **B** – tooth is **deciduous**.
- **C – crown**.
- **E – resin** filling material.
- **G – gold** restoration.
- **H – porcelain**.
- **N – non-precious** filling or crown material. Includes stainless steal.
- **P – pontic**. Primary code must be X to indicate missing tooth.
- **R – root canal** filled.
- **S** – silver amalgam.
- **T** – denture tooth. Primary code must be X to indicate missing tooth.
- **Z** – temporary filling material. Also indicates gross caries (used sparingly).

Figure 1.3: WinID dental codes - extensions of CAPMI dental codes

Examples

- **MODFL-S** mesial occlusal distal facial lingual silver amalgam restoration.
- **DL** tooth has distal lingual restoration
- **MODFL-CG** gold crown.
- **MODFL-CHR** endodontically treated tooth with porcelain crown.
- **MI-E** mesial incisal resin.
- **X** tooth missing.
- **V-B** virgin deciduous tooth.
- **MO-SB** mesial occlusal silver amalgam in deciduous tooth.
- **X-PN** missing tooth replaced with non-precious pontic.
- **X-T** missing tooth replaced with denture tooth.
- **J** missing postmortem.
- **MO-AZ** mesial occlusal temporary filling (or caries) on tooth with anomaly.

Figure 1.4: An example of the dental chart entry in an individual's record

root contours are not charted. However, it is expected that future generations will experience less dental decay, giving forensic odontologists very little information to work with. Furthermore, modern dental material used for filings and restorations produces poor quality radiographs, complicating the process of dental charting. Consequently, a shift towards a comparison system based on morphology of crowns and roots is necessary [14, 15, 8].

The coding, extraction and matching process for NCIC, WinID and CAPMI are done manually. An obvious disadvantage of this approach is that it is error prone and time consuming. A person preparing PM and AM records carefully examines and documents morphology of each tooth present in a radiograph. Even a single typographic mistake will lead to an erroneous record, possibly eliminating the correct match. Additionally, relative interpretation of x-rays results in observational findings that might not necessarily be agreed upon by all observers. Since the interpretation of records is rather subjective, the strength of a match between a PM and AM dental chart could be affected by the clinical experience level of the forensic odontologist. Furthermore, the information contained within the image itself, is never used in dental matching. The entire search and match process is purely text-based.

1.2.3 Current Research

In the past few years, Michigan State University, West Virginia University and the University of Miami jointly attempted to address the problem of developing an automated system for postmortem identification using dental radiographs. The prototype for the Automated Dental Identification System (ADIS) was first presented in 2003 [8, 16]. Shortly after, Jain, Chen and Minut implemented a semi-automatic method that extracts the shapes of teeth from AM and PM radiographs [5, 17, 18]. The proposed method involves radiograph segmentation, pixel classification and contour matching. The teeth are matched by shape fitting, and scores are ranked by the distance between the PM and AM shapes. The method was tested using 39 query images on a database of 130 images. For a total of 25 out of 39

queries, the correct AM images were ranked first. Zhou and Mottaleb aimed at enabling content-based retrieval of AM radiographs that have similar tooth contours compared to a given PM radiograph [19, 20, 21]. Radiographs are classified by their type (panoramic, periapical and bitewing), and teeth in bitewing images are segmented and stored in the database. The method retrieves radiographs from the AM database based on the Hausdorff distance measure between the tooth contours. Mottaleb and Mahoor continued work on classification and numbering of teeth in bitewing images [22], and reported a 90% accuracy of tooth classification. Jain and Chen improved the originally- proposed tooth contour extraction method by using directional snakes to discriminate boundaries between the adjacent teeth [23], and since have moved towards using the human dental atlas for registration [24]. They are currently working on using the indices of teeth to match two radiographs for human identification. Most of the research involving radiographic registration for identification purposes strongly focuses and relies on the automatic segmentation of the tooth's image.

1.3 Thesis Statement

The objective of this research is to propose a computer-aided framework for efficient matching of dental radiographs for human identification purposes. Given a PM radiograph with a marked region of interest (ROI), we search the database of AM radiographs to retrieve a closest match with respect to the ROI. The key contribution here is the application of the Weighted Sum of Squared Differences (SSD) cost function as a similarity measure in this problem domain. The SSD cost function was slightly modified to account for the possibility of radiographs being acquired at different angles, as well as teeth shifting and rotating over time. The operation of rotation is linearly approximated, and thus is valid over a limited range of angles. Efficient evaluation of SSD using the Discrete Fourier Transform (DFT) makes it feasible to simultaneously find the locally optimal rotation, and globally optimal alignment, brightness and contrast adjustment between the two radiographs. Experimental results indicate that matching dental records using SSD

is a viable method for human identification purposes.

1.4 Organization of the Thesis

The remainder of the thesis is organized as follows. In Chapter 2 we outline error metrics used in image matching and provide the in-depth description of the Weighted Sum of Squared Differences cost function. The optimization of the SSD using the Discrete Fourier Transform is described. In Chapter 3 we describe how we incorporated rotation into the SSD cost function to accurately reflect the nature of the dental x-rays matching problem. Chapters 4 and 5 describe the process of data acquisition, experiments and discuss obtained results. Chapter 6 presents the conclusions and future work.

Chapter 2

Image Matching

Image matching refers to a process of estimating an optimal transformation that brings two images into spatial alignment. Images could be related through a non-rigid or rigid-body transformation. A rigid-body transformation is a mapping that preserves distances between points. Translation, rotation, and combinations thereof are examples of rigid-body transformations. Non-rigid transformations, such as shears, dilations and other more complex distortions, do not necessarily preserve distances between points. In this thesis, we focus only on rigid-body transformations.

In order to match two images we need to define an appropriate similarity measure. A similarity measure is used to evaluate the spatial correspondence of images and it should be suited to the optimization method used for the alignment (matching).

2.1 The Error Metrics

When determining the appropriate error metric, we have to take into consideration the method used for the alignment. Some methods perform image matching over an entire image, while others use only a portion of an image, usually referred to as

a region of interest (ROI). Within the scope of this thesis, only a part of the image is used for matching. While the AM and PM dental x-rays may depict the same tooth, or even several teeth, it is highly unlikely that they will be exactly the same. Thus, matching over an entire image would not provide the desired results and we have to consider an alignment over a specified ROI.

In image processing, several different methods are used for registration. A common image similarity measure is Pearson's cross-correlation coefficient [25]. The cross-correlation coefficient is defined as

$$C(a) = \frac{\int f(x)g(x-a)dx}{\sqrt{\int f^2(x)dx \int g^2(x)dx}} \ . \tag{2.1}$$

The measure of correlation between the functions $f(x)$ and $g(x-a)$ is given by $C(a)$. If g and f are equal, the $C(a)$ achieves its maximum value when there is no shift, meaning the corresponding value of $a = 0$.

The correlation coefficient cost function is commonly used for within-modality image registration problems. However, this type of cost function is restricted in a sense that, although it considers contrast changes, it cannot account for brightness adjustments. It is unrealistic to expect that two x-rays will have the same brightness and contrast properties. Consequently, we need to explore a possibility of a better suited error metric that takes into account these properties while matching the images.

Entropy-based similarity measures originating from information theory, such as mutual information and normalized mutual information [26, 27, 28, 29, 30] are common in both monomodal (same modality) and multimodal (different modalities) registration scenarios. Mutual information is a quantity that measures the mutual dependence of the two variables. Formally, mutual information is defined as

$$I(X;Y) = \sum_{y \in Y} \sum_{x \in X} p(x,y) \log \frac{p(x,y)}{p(x)p(y)} \tag{2.2}$$

where $p(x)$ and $p(y)$ are the marginal probability density functions of X and Y respectively, while $p(x,y)$ is the joint probability density function of X and Y. In

the context of image registration, x is an intensity value from one image, while y is an intensity value from the other. Then $p(x)$ and $p(y)$ can be estimated from the intensity histograms of the images. Similarly, $p(x, y)$ can be estimated from the joint intensity histogram.

Mutual information can be equivalently expressed as a difference between the marginal entropies contained in each image over the ROI and the joint entropy contained in the overlayed images over the ROI,

$$I(X;Y) = H(X) + H(Y) - H(X,Y) \ . \tag{2.3}$$

Quantities $H(X)$ and $H(Y)$ represent marginal entropies of X and Y respectively, while $H(X,Y)$ represents the joint entropy of X and Y. Image registration is performed by maximizing the mutual information.

The advantage of mutual information methods is that they make no assumption about the form of the intensity mapping between the two images; merely that regions with matching intensities in one image are likely to have similar intensities in the other image.

Mutual information has its drawbacks. Since there is no known way to efficiently perform an exhaustive search over parameter space, registration problems using mutual information are computationally expensive. Thus, implementations rely heavily on optimization methods. Additionally, the process of estimating the joint probability density function requires binning of pixels into discrete categories, giving the cost function discontinuities. In [31] and [32] it was shown that mutual information performs poorly when the initial misregistration is large compared to the size of the ROI (which could be a case with dental x-rays). It is unrealistic to assume that the chosen tooth in the PM image is nearly aligned with the corresponding tooth in the AM image.

There are some methods that are capable of finding a global optimum for registration [33, 34, 35], but these methods typically must use the whole image, and cannot work with an ROI. The fact that we are registering only within a small ROI leads us to the Weighted Sum of Squared Differences (SSD) cost function.

2.1.1 Weighted Sum of Squared Differences

The Weighted Sum of Squared Differences cost function allows us to find an optimal shift for the alignment of image $\mathbf{f}$ to image $\mathbf{g}$, while incorporating a weighting function $\mathbf{w}$. The weighting function $\mathbf{w}$, also commonly referred to as an 'alpha channel' [36] or 'alpha map' [37], is used to specify the ROI over which the matching of two images $\mathbf{f}$ and $\mathbf{g}$ will take place. The common implementation of a weighting function is a piecewise constant function with values 1 inside the ROI, and 0 elsewhere.

Given the $M \times N$ images $\mathbf{f}$, $\mathbf{g}$ and $\mathbf{w}$, the weighted SSD cost function is

$$\mathbf{C} = \sum_{m=0}^{M-1} \sum_{n=0}^{N-1} \left[\mathbf{f}_{m,n} - \mathbf{g}_{m,n}\right]^2 \mathbf{w}_{m,n} \ , \tag{2.4}$$

where $\mathbf{f}_{m,n}$ refers to the intensity of pixel (m, n) in the image $\mathbf{f}$ (likewise for $\mathbf{g}_{m,n}$ and $\mathbf{w}_{m,n}$). To match the translated image $\mathbf{f}$ to $\mathbf{g}$, we have to find the parameters a and b that minimize

$$\mathbf{C}(a, b) = \sum_{m=0}^{M-1} \sum_{n=0}^{N-1} \left[\mathbf{f}_{m-a,n-b} - \mathbf{g}_{m,n}\right]^2 \mathbf{w}_{m,n} \ . \tag{2.5}$$

2.1.2 Intensity-Remapped SSD

The SSD cost function given in (2.5) assumes that the intensity mappings for $\mathbf{f}$ and $\mathbf{g}$ are the same. However, in the context of this research, we can not make that assumption. Dental x-rays $\mathbf{f}$ and $\mathbf{g}$ could have come from different acquisition or rendering processes (i.e. digital vs. standard radiography) or could have even been processed differently. Consequently, they could represent the same scene using different greytones or intensities. To account for this, we extended (2.5) by replacing $\mathbf{f}$ with $s_0 + s_1\mathbf{f}$. In [38], it was shown that in conjunction to finding the optimal translation, the globally optimal contrast and brightness adjustment can be computed efficiently by finding values a, b, s_0 and s_1 that minimize

$$\mathbf{C}(a, b, s_0, s_1) = \sum_{m=0}^{M-1} \sum_{n=0}^{N-1} \left[(s_0 + s_1\mathbf{f}_{m-a,n-b}) - \mathbf{g}_{m,n}\right]^2 \mathbf{w}_{m,n} \ . \tag{2.6}$$

Expanding the brackets in (2.6) we obtain

$$\begin{aligned}\mathbf{C}(a,b,s_0,s_1) &= \sum_{m=0}^{M-1}\sum_{n=0}^{N-1} s_0^2\mathbf{w}_{m,n} + 2\sum_{m=0}^{M-1}\sum_{n=0}^{N-1} s_0 s_1 \mathbf{f}_{m-a,n-b}\mathbf{w}_{m,n} \\ &+ \sum_{m=0}^{M-1}\sum_{n=0}^{N-1} s_1^2\mathbf{f}_{m-a,n-b}^2\mathbf{w}_{m,n} - 2\sum_{m=0}^{M-1}\sum_{n=0}^{N-1} s_0\mathbf{g}_{m,n}\mathbf{w}_{m,n} \\ &- 2\sum_{m=0}^{M-1}\sum_{n=0}^{N-1} s_1\mathbf{f}_{m-a,n-b}\mathbf{g}_{m,n}\mathbf{w}_{m,n} + \sum_{m=0}^{M-1}\sum_{n=0}^{N-1}\mathbf{g}_{m,n}^2\mathbf{w}_{m,n}\ .\end{aligned} \tag{2.7}$$

Since s_0 and s_1 are not functions of m and n, they can be factored out of the summations in (2.7) leading to

$$\begin{aligned}\mathbf{C}(a,b,s_0,s_1) &= s_0^2\sum_{m=0}^{M-1}\sum_{n=0}^{N-1}\mathbf{w}_{m,n} + 2s_0 s_1\sum_{m=0}^{M-1}\sum_{n=0}^{N-1}\mathbf{f}_{m-a,n-b}\mathbf{w}_{m,n} \\ &+ s_1^2\sum_{m=0}^{M-1}\sum_{n=0}^{N-1}\mathbf{f}_{m-a,n-b}^2\mathbf{w}_{m,n} - 2s_0\sum_{m=0}^{M-1}\sum_{n=0}^{N-1}\mathbf{g}_{m,n}\mathbf{w}_{m,n} \\ &+ \sum_{m=0}^{M-1}\sum_{n=0}^{N-1}\mathbf{g}_{m,n}^2\mathbf{w}_{m,n} - 2s_1\sum_{m=0}^{M-1}\sum_{n=0}^{N-1}\mathbf{f}_{m-a,n-b}\mathbf{g}_{m,n}\mathbf{w}_{m,n}\ .\end{aligned} \tag{2.8}$$

The summations of the first, fourth and fifth terms in (2.8) are all constant with the respect to a and b, and can easily be computed in linear ($\mathcal{O}(NM)$) time. However, direct evaluation of the remaining summation terms in (2.8) for all possible integer shifts (a,b) is expensive and requires ($\mathcal{O}(N^2M^2)$) floating point operations (flops).

2.2 Optimization

For the remainder of this thesis we make the assumption that the images are periodic; they repeat infinitely. Given an $M \times N$ image, we assume that $\mathbf{f}_{m,n} = \mathbf{f}_{m+M,n} = \mathbf{f}_{m,n+N}$.

Consider the second summation term in (2.8),

$$\sum_{m=0}^{M-1}\sum_{n=0}^{N-1}\mathbf{f}_{m-a,n-b}\mathbf{w}_{m,n}\ . \tag{2.9}$$

It can be reformulated into a convolution,

$$\sum_{m=0}^{M-1}\sum_{n=0}^{N-1}\bar{\mathbf{f}}_{a-m,b-n}\mathbf{w}_{m,n} \quad = \quad (\bar{\mathbf{f}} \star \mathbf{w})_{a,b} \ , \tag{2.10}$$

where $\bar{\mathbf{f}}$ is a reflected version of $\mathbf{f}$, such that $\bar{\mathbf{f}}_{i,j} = \mathbf{f}_{-i,-j}$. It was shown by [38, 39] that evaluating (2.10) in the frequency domain reduces the computational time complexity from $\mathcal{O}(N^2M^2)$ to $\mathcal{O}(MN\log(MN))$ flops. Convolution in the image (spatial) domain is equivalent to element-wise multiplication in the frequency domain and can be evaluated efficiently using the Fast Fourier Transform (FFT). Details on how this is done are described in the following section.

2.2.1 Discrete Fourier Transform

The Fourier Transform is an important image processing tool. The essence of the FT is to represent a function ('signal') in the frequency domain. In other words, the Fourier Transform decomposes the signal into the weighted sum of sinusoids of different frequencies [40]. The main benefit of this transform is the intuitive interpretation of weights as a frequency decomposition of the input signal. Each weight, called a Fourier coefficient, corresponds to a phase, frequency and amplitude of a sinusoid. The collection of Fourier coefficients is the frequency domain representation of the signal, containing the same information as the original signal, differing from it only in the manner of the representation of the information. Adding up all sinusoids for all the Fourier coefficients reconstructs the original signal.

The version of FT that operates on discrete (sampled) data is called a Discrete Fourier Transform (DFT). The DFT is an invertible transformation that converts a sequence of N complex numbers $\{\mathbf{f}_n \mid n = 0, ..., N-1\}$, into another sequence of N complex numbers $\{\mathbf{F}_k \mid k = 0, ..., N-1\}$. In this context, we refer to $\mathbf{f}$ as the spatial domain signal, and $\mathbf{F}$ as the frequency domain signal. Additionally, we refer to $\mathbf{F}_k$ as a Fourier coefficient. Since we are working with images, we will assume for the duration of this thesis that $\mathbf{f}$ is a real-valued signal (i.e. the imaginary part is zero). Since the DFT is invertible, we can convert between $\mathbf{f}_n$ and $\mathbf{F}_k$ without loss of information.

As mentioned, the Fourier Transform works by decomposing a signal into its sine and cosine components, where each point in the frequency domain represents a particular frequency contained in the spatial domain signal. Since these trigonometric components form an orthonormal basis, finding the Fourier coefficients of $\mathbf{f}$ is simply a matter of computing

$$a_k = \frac{1}{N}\sum_{n=0}^{N-1} \mathbf{f}_n \cos(kt_n) \tag{2.11}$$

$$b_k = \frac{1}{N}\sum_{n=0}^{N-1} \mathbf{f}_n \sin(kt_n) \tag{2.12}$$

for $k = 0, ..., N-1$, where the points $t_n = n\frac{2\pi}{N}$ are evenly spaced on an interval $[0, 2\pi)$.

If we combine a_k and b_k into a single complex number $\mathbf{F}_k = a_k + ib_k$ then the DFT can be written

$$\mathbf{F}_k = \frac{1}{N}\sum_{n=0}^{N-1} \mathbf{f}_n[\cos(kt_n) + i\sin(kt_n)] \ . \tag{2.13}$$

Using Euler's formula relating the trigonometric and exponential functions for complex values

$$e^{ix} = \cos(x) + i\sin(x) \tag{2.14}$$

the Fourier coefficient $\mathbf{F}_k$ can be defined as

$$\mathbf{F}_k = \frac{1}{N}\sum_{n=0}^{N-1} \mathbf{f}_n e^{\frac{-2\pi ink}{N}} \tag{2.15}$$

giving us the definition of the Discrete Fourier Transform.

2.2.2 Inverse Discrete Fourier Transform

The Inverse Discrete Fourier Transform (IDFT) is defined as

$$\mathbf{f}_n = \sum_{n=0}^{N-1} F_k e^{\frac{2\pi ink}{N}} \ . \tag{2.16}$$

This inverse transformation allows us to determine the spatial domain function from its Fourier coefficients. If the 'signals' or 'sequences' $\mathbf{F}_k$ and $\mathbf{f}_n$ are related by equations (2.15) and (2.16) then they are termed a *Fourier Transform pair*.

2.2.3 2D Fourier Transform

Since we are utilizing the Fourier Transform for image processing, we need to provide a definition of the DFT and IDFT for a two-dimensional (2D) signal. The DFT of a 2D function $\mathbf{f}_{m,n}$ is another 2D function defined as

$$\mathbf{F}_{j,k} = \sum_{j=0}^{M-1} \sum_{k=0}^{N-1} \mathbf{f}_{m,n} e^{-2\pi i (j\frac{m}{M} + k\frac{n}{N})} \tag{2.17}$$

$$j \in [0, ..., M-1], k \in [0, ..., N-1] \ . \tag{2.18}$$

The IDFT of a 2D function $\mathbf{F}_{j,k}$ is defined as

$$\mathbf{f}_{m,n} = \frac{1}{MN} \sum_{m=0}^{M-1} \sum_{n=0}^{N-1} \mathbf{F}_{j,k} e^{2\pi i (j\frac{m}{M} + k\frac{n}{N})} \tag{2.19}$$

$$m \in [0, ..., M-1], n \in [0, ..., N-1] \ . \tag{2.20}$$

2.2.4 Convolution Theorem

The Fourier Transform's treatment of convolution is considered a fundamental tool in image processing. In a discrete 2D space, convolution of two discrete signals $\mathbf{f}_{m,n}$ and $\mathbf{g}_{m,n}$, where $m = 0, ..., M-1$ and $n = 0, ..., N-1$, is defined as

$$(\mathbf{f} \star \mathbf{g})_{a,b} = \sum_{m=0}^{M-1} \sum_{n=0}^{N-1} \mathbf{f}_{m,n} \mathbf{g}_{a-m,b-n} \ . \tag{2.21}$$

$$a \in [0, ..., M-1], b \in [0, ..., N-1] \ , \tag{2.22}$$

where the ranges of a and b reflect the fact that f and g are assumed to be periodic. It is well known that the convolution in the spatial (image) domain is equivalent to element-wise multiplication in the frequency domain [40]

$$DFT(\mathbf{f} \star \mathbf{g})_{j,k} = \mathbf{F}_{j,k}\mathbf{G}_{j,k} \ . \tag{2.23}$$

Due to this property, the evaluation of (2.10) in the frequency domain reduces the computational time complexity from $\mathcal{O}(N^2M^2)$ to $\mathcal{O}(MN\log(MN))$ flops.

Chapter 3

Method

It was shown by Orchard [38] that in addition to finding the optimal match over all possible integer shifts, we can also efficiently find an optimal match over all linear intensity remappings. When matching two dental radiographs, we are looking for both the shift that best aligns the two radiographs over the given region of interest (ROI), as well as the best contrast and brightness adjustment that makes the corresponding parts of the two radiographs as similar as possible. As shown in Chapter 2, optimal alignment and intensity remapping is given by parameters a, b, s_0 and s_1 that minimize

$$\mathbf{C}(m, n, s_0, s_1) = \sum_{m=0}^{M-1} \sum_{n=0}^{N-1} \left[s_0 + s_1 \mathbf{f}_{m-a,n-b} - \mathbf{g}_{m,n} \right]^2 \mathbf{w}_{m,n} \ . \tag{3.1}$$

However, (3.1) does not account for rotations. Since teeth naturally shift and rotate over time, the cost function needs to be extended to incorporate this aspect. Furthermore, radiographs can be obtained at different angles of acquisition, resulting in slightly rotated depictions of the same tooth.

3.1 Modeling Rotation

To extend (3.1), we model rotation using a linear approximation

$$\mathbf{R}(\mathbf{f}, \theta) \approx \mathbf{f} + \mathbf{J}\theta \ , \tag{3.2}$$

where $\mathbf{J}$ holds the derivatives of $\mathbf{f}$ with respect to rotation parameters. Substituting (3.2) into (3.1) yields

$$\begin{aligned}
\mathbf{C}(a, b, s_0, s_1) &= \sum_{m=0}^{M-1} \sum_{n=0}^{N-1} \left[s_0 + s_1 R(\mathbf{f}, \theta)_{m-a,n-b} - \mathbf{g}_{m,n} \right]^2 \mathbf{w}_{m,n} \\
&= \sum_{m=0}^{M-1} \sum_{n=0}^{N-1} \left[s_0 + s_1 (\mathbf{f}_{m-a,n-b} + \mathbf{J}_{m-a,n-b}\theta) - \mathbf{g}_{m,n} \right]^2 \mathbf{w}_{m,n} \qquad (3.3) \\
&= \sum_{m=0}^{M-1} \sum_{n=0}^{N-1} \left[s_0 + s_1 \mathbf{f}_{m-a,n-b} + s_2 \mathbf{J}_{m-a,n-b} - \mathbf{g}_{m,n} \right]^2 \mathbf{w}_{m,n}
\end{aligned}$$

where $s_2 = s_1\theta$. To simplify the notation, let

$$\begin{aligned}
\mathbf{F} &= \mathbf{f}_{m-a,n-b} && (3.4) \\
\mathbf{G} &= \mathbf{g}_{m,n} && (3.5) \\
\mathbf{W} &= \mathbf{w}_{m,n} && (3.6) \\
\mathbf{J} &= \mathbf{J}_{m-a,n-b} \ . && (3.7)
\end{aligned}$$

Then (3.3) can be written

$$\mathbf{C}(a, b, s_0, s_1, s_2) = \sum_{m=0}^{M-1} \sum_{n=0}^{N-1} (s_0 + s_1\mathbf{F} + s_2\mathbf{J} - \mathbf{G})^2\mathbf{W} \ . \tag{3.8}$$

Multiplying out the terms and expanding the brackets results in

$$\begin{aligned}
\mathbf{C}(a, b, s_0, s_1, s_2) = \sum_{m=0}^{M-1} \sum_{n=0}^{N-1} \big(& s_0^2\mathbf{W} + 2s_0s_1\mathbf{F}\mathbf{W} + s_1^2\mathbf{F}^2\mathbf{W} + 2s_0s_2\mathbf{J}\mathbf{W} \\
& -2s_0\mathbf{G}\mathbf{W} + 2s_1s_2\mathbf{F}\mathbf{J}\mathbf{W} - 2s_1\mathbf{F}\mathbf{G}\mathbf{W} \qquad (3.9) \\
& +s_2^2\mathbf{J}^2\mathbf{W} - 2s_2\mathbf{J}\mathbf{G}\mathbf{W} + \mathbf{G}^2\mathbf{W} \big) \ .
\end{aligned}$$

Simplifying our notation further, and defining

$$\mathbf{e}_1 = \sum_{m=0}^{M-1}\sum_{n=0}^{N-1} \mathbf{w}_{m,n} \tag{3.10}$$

$$\mathbf{e}_2 = \sum_{m=0}^{M-1}\sum_{n=0}^{N-1} \mathbf{f}_{m-a,n-b}\mathbf{w}_{m,n} \tag{3.11}$$

$$\mathbf{e}_3 = \sum_{m=0}^{M-1}\sum_{n=0}^{N-1} \mathbf{f}^2_{m-a,n-b}\mathbf{w}_{m,n} \tag{3.12}$$

$$\mathbf{e}_4 = \sum_{m=0}^{M-1}\sum_{n=0}^{N-1} \mathbf{J}_{m-a,n-b}\mathbf{w}_{m,n} \tag{3.13}$$

$$\mathbf{e}_5 = \sum_{m=0}^{M-1}\sum_{n=0}^{N-1} \mathbf{g}_{m,n}\mathbf{w}_{m,n} \tag{3.14}$$

$$\mathbf{e}_6 = \sum_{m=0}^{M-1}\sum_{n=0}^{N-1} \mathbf{f}_{m-a,n-b}\mathbf{J}_{m-a,n-b}\mathbf{w}_{m,n} \tag{3.15}$$

$$\mathbf{e}_7 = \sum_{m=0}^{M-1}\sum_{n=0}^{N-1} \mathbf{f}_{m-a,n-b}\mathbf{g}_{m,n}\mathbf{w}_{m,n} \tag{3.16}$$

$$\mathbf{e}_8 = \sum_{m=0}^{M-1}\sum_{n=0}^{N-1} \mathbf{J}^2_{m-a,n-b}\mathbf{w}_{m,n} \tag{3.17}$$

$$\mathbf{e}_9 = \sum_{m=0}^{M-1}\sum_{n=0}^{N-1} \mathbf{J}_{m-a,n-b}\mathbf{g}_{m,n}\mathbf{w}_{m,n} \tag{3.18}$$

$$\mathbf{e}_{10} = \sum_{m=0}^{M-1}\sum_{n=0}^{N-1} \mathbf{g}^2_{m,n}\mathbf{w}_{m,n} \tag{3.19}$$

the right-hand side of the equation (3.9) becomes

$$s_0^2\mathbf{e}_1 + 2s_0s_1\mathbf{e}_2 + s_1^2\mathbf{e}_3 + 2s_0s_2\mathbf{e}_4 - 2s_0\mathbf{e}_5 + 2s_1s_2\mathbf{e}_6 - 2s_1\mathbf{e}_7 + s_2^2\mathbf{e}_8 - 2s_2\mathbf{e}_9 + \mathbf{e}_{10}\ . \tag{3.20}$$

3.2 Determining the minimum

While it is not explicitly stated, the coefficients s_0, s_1 and s_2 are functions of the shift, a and b. That is, we can compute a different optimal set of coefficients for

each candidate shift. As such, our strategy for optimizing (3.20) is to efficiently compute the optimal coefficients for all possible shifts. In the previous section, we described how the summations could efficiently be computed for all possible shifts. In this section, we describe how, for a given shift, to find the optimal coefficients, s_0, s_1, and s_2. The minimum value of (3.20) can be determined by taking the partial derivatives of (3.20) with respect to s_0, s_1 and s_2 and setting them to 0,

$$\begin{aligned} 2s_0\mathbf{e}_1 + 2s_1\mathbf{e}_2 + 2s_2\mathbf{e}_4 - 2\mathbf{e}_5 &= 0 \\ 2s_0\mathbf{e}_2 + 2s_1\mathbf{e}_3 + 2s_2\mathbf{e}_6 - 2\mathbf{e}_7 &= 0 \\ 2s_0\mathbf{e}_4 + 2s_1\mathbf{e}_6 + 2s_2\mathbf{e}_8 - 2\mathbf{e}_9 &= 0 \end{aligned} \tag{3.21}$$

which leads to a simple 3×3 system of linear equations.

Solving (3.21) yields the following values for s_0, s_1 and s_2

$$s_0 = \frac{\mathbf{e}_2\mathbf{e}_6\mathbf{e}_9 - \mathbf{e}_2\mathbf{e}_7\mathbf{e}_8 - \mathbf{e}_4\mathbf{e}_3\mathbf{e}_9 + \mathbf{e}_4\mathbf{e}_6\mathbf{e}_7 + \mathbf{e}_3\mathbf{e}_5\mathbf{e}_8 - \mathbf{e}_5\mathbf{e}_6^2}{2\mathbf{e}_2\mathbf{e}_4\mathbf{e}_6 + \mathbf{e}_1\mathbf{e}_3\mathbf{e}_8 - \mathbf{e}_1\mathbf{e}_6^2 - \mathbf{e}_2^2\mathbf{e}_8 - \mathbf{e}_3\mathbf{e}_4^2} \tag{3.22}$$

$$s_1 = \frac{\mathbf{e}_1\mathbf{e}_7\mathbf{e}_8 + \mathbf{e}_2\mathbf{e}_4\mathbf{e}_9 - \mathbf{e}_1\mathbf{e}_6\mathbf{e}_9 + \mathbf{e}_4\mathbf{e}_5\mathbf{e}_6 - \mathbf{e}_2\mathbf{e}_5\mathbf{e}_8 - \mathbf{e}_7\mathbf{e}_4^2}{2\mathbf{e}_2\mathbf{e}_4\mathbf{e}_6 + \mathbf{e}_1\mathbf{e}_3\mathbf{e}_8 - \mathbf{e}_1\mathbf{e}_6^2 - \mathbf{e}_2^2\mathbf{e}_8 - \mathbf{e}_3\mathbf{e}_4^2} \tag{3.23}$$

$$s_2 = \frac{\mathbf{e}_2\mathbf{e}_4\mathbf{e}_7 + \mathbf{e}_2\mathbf{e}_5\mathbf{e}_6 + \mathbf{e}_1\mathbf{e}_3\mathbf{e}_9 - \mathbf{e}_3\mathbf{e}_4\mathbf{e}_5 - \mathbf{e}_1\mathbf{e}_6\mathbf{e}_7 - \mathbf{e}_9\mathbf{e}_2^2}{2\mathbf{e}_2\mathbf{e}_4\mathbf{e}_6 + \mathbf{e}_1\mathbf{e}_3\mathbf{e}_8 - \mathbf{e}_1\mathbf{e}_6^2 - \mathbf{e}_2^2\mathbf{e}_8 - \mathbf{e}_3\mathbf{e}_4^2} \,. \tag{3.24}$$

Chapter 4

Experiments

The method was implemented in MATLAB (*MathWorks Inc., Natick, Massachusetts*) and tested on a database of 571 dental radiographs belonging to 41 distinct individuals (also referred to as 'subjects'). Each subject had a dental record consisting of two or more radiographs. Here, we define a dental record as a set of radiographs collected during a single session (visit to the dentist). Exactly 21 subjects had multiple dental records obtained at different times, i.e. one record obtained in a 1982 session, and a subsequent record obtained in 1984.

All radiographs were scanned using a backlit scanner at a resolution of 800 dpi, and saved in a JPEG format with a quality factor of 100. To address privacy issues associated with this type of data, all individuals were assigned a unique patient number ranging from 1 to 41. Each scanned image was then identified using the patient number, followed by the session number and the image number. For example, the image 'P25_S02_05.jpg' would identify a $5th$ dental radiograph belonging to the patient number 25, obtained in the $2nd$ session. The AM database consisted of these scanned images.

A total of 125 of the most recent dental radiographs belonging to subjects with multiple sessions were treated as PM images. For each of the PM radiographs, an ROI was defined by roughly encompassing a tooth over which we wanted to perform a matching process. Pixels of interest were given a weight of 1, while all other pixels

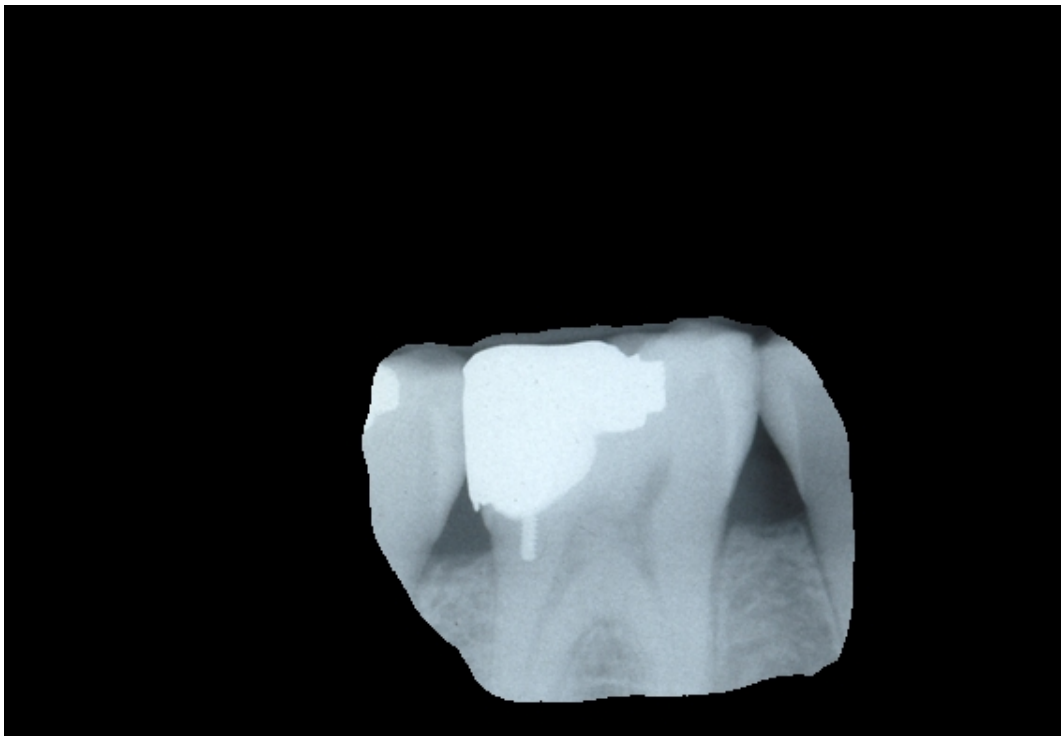

Figure 4.1: Contents of the ROI for a single radiograph

were assigned a weight of 0. Small regions surrounding the tooth (whether it be a neighboring tooth or a dark portion of the radiograph), were also included in the ROI. Figure 4.1 shows the contents of the ROI for a single radiograph. For some radiographs, more than one ROI was defined resulting in a total of 150 test cases.

Given a PM radiograph with an ROI, our goal is to determine the identity of the person by retrieving the closest match from the AM database. Note, however, that PM radiographs were not permanently removed from the database, but rather excluded for the appropriate test case. Figure 4.2 illustrates the process. If we were to remove the PM radiographs, the size of the database would be reduced from 571 to 446 radiographs. Maintaining the size of the database was important as it allowed us to have more AM to PM/ROI matching pairs. Thus, each identification trial then consisted of removing one of the PM sessions from the database and matching

one of its images (with an associated ROI) to all the remaining images in the AM database.

Using our method, the PM/ROI image is matched pixel by pixel against all the remaining images in the database. For all possible shifts, the best intensity remapping (and hence, the best small rotation) is computed, and the minimum parameters, along with the associated error (cost), are recorded. An overview of the approach is shown in Fig. 4.3. The radiographs in the database are then ranked according to the error, with the smallest error indicating the best match.

For example, matching a PM/ROI pair depicted in Figure 4.1, to a small database consisting of 25 AM radiographs produces results shown in Fig. 4.4. As can be seen in Fig. 4.5, the top ranked match was the correct one. Our method works by finding the best shift, brightness and contrast adjustment as well as small rotation that minimize the cost function and consequently bring two radiographs into alignment. The process is illustrated by two sample images depicted in Fig. 4.6. The area of overlap between the two images is outlined in red. Translating the image on the left by $[x, y]$, and rotating it by θ, where x,y, and θ parameters are determined by our method, we achieve an overlap depicted in Fig. 4.7. The difference image shown in Fig. 4.8 illustrates the quality of the registration.

In the scope of this work, two separate scenarios are considered, each consisting of 150 test cases, for a total of 300 tests. Both scenarios use a single ROI in the process of matching. One scenario was tested on a database of radiographs approximately sized at 550×380, and another on radiographs approximately sized at 225×190.

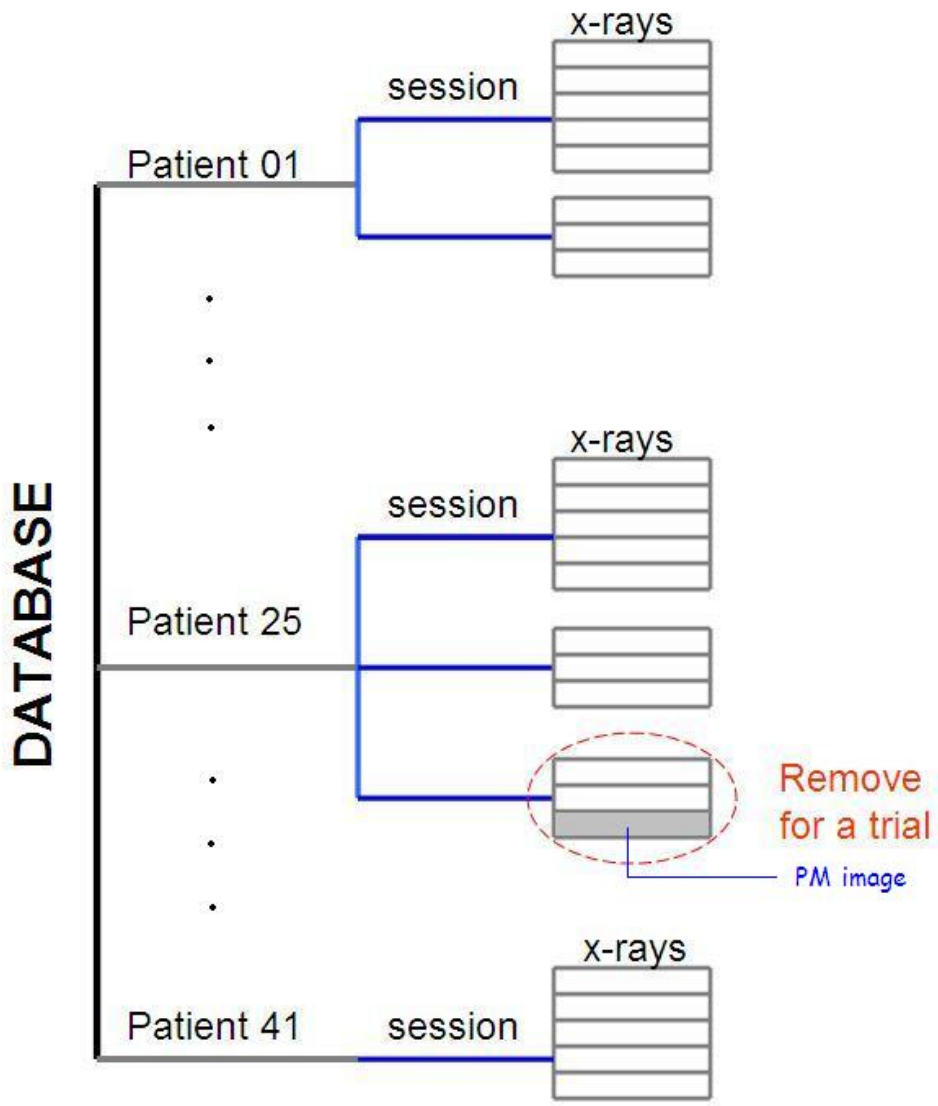

Figure 4.2: Illustration of an identification test run

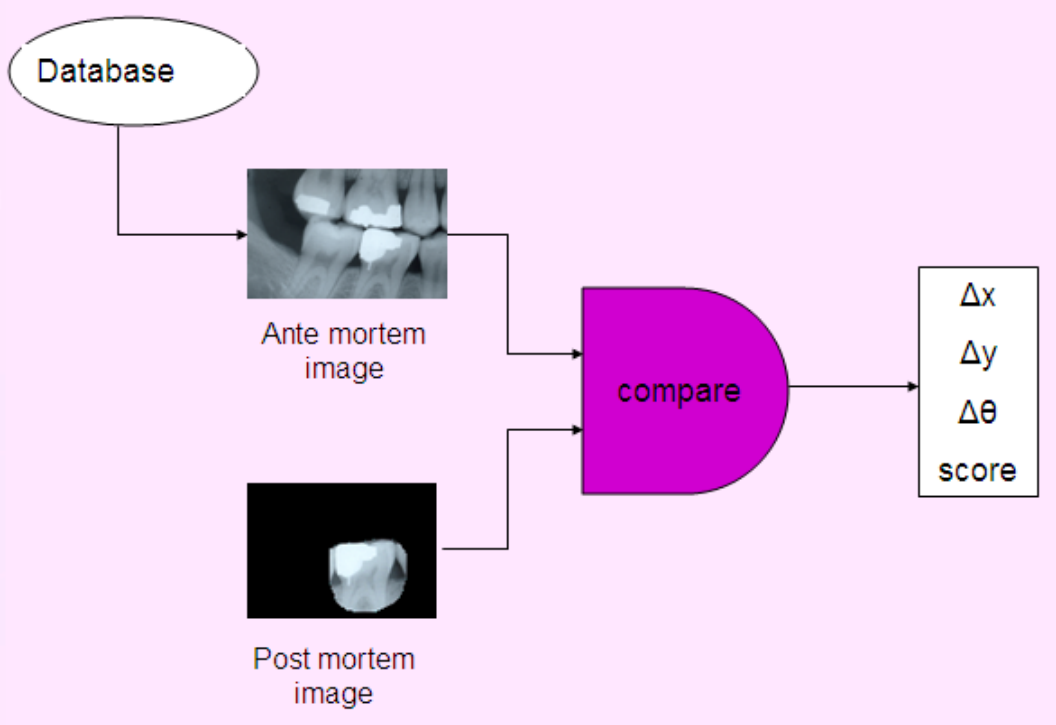

Figure 4.3: Overview of the approach

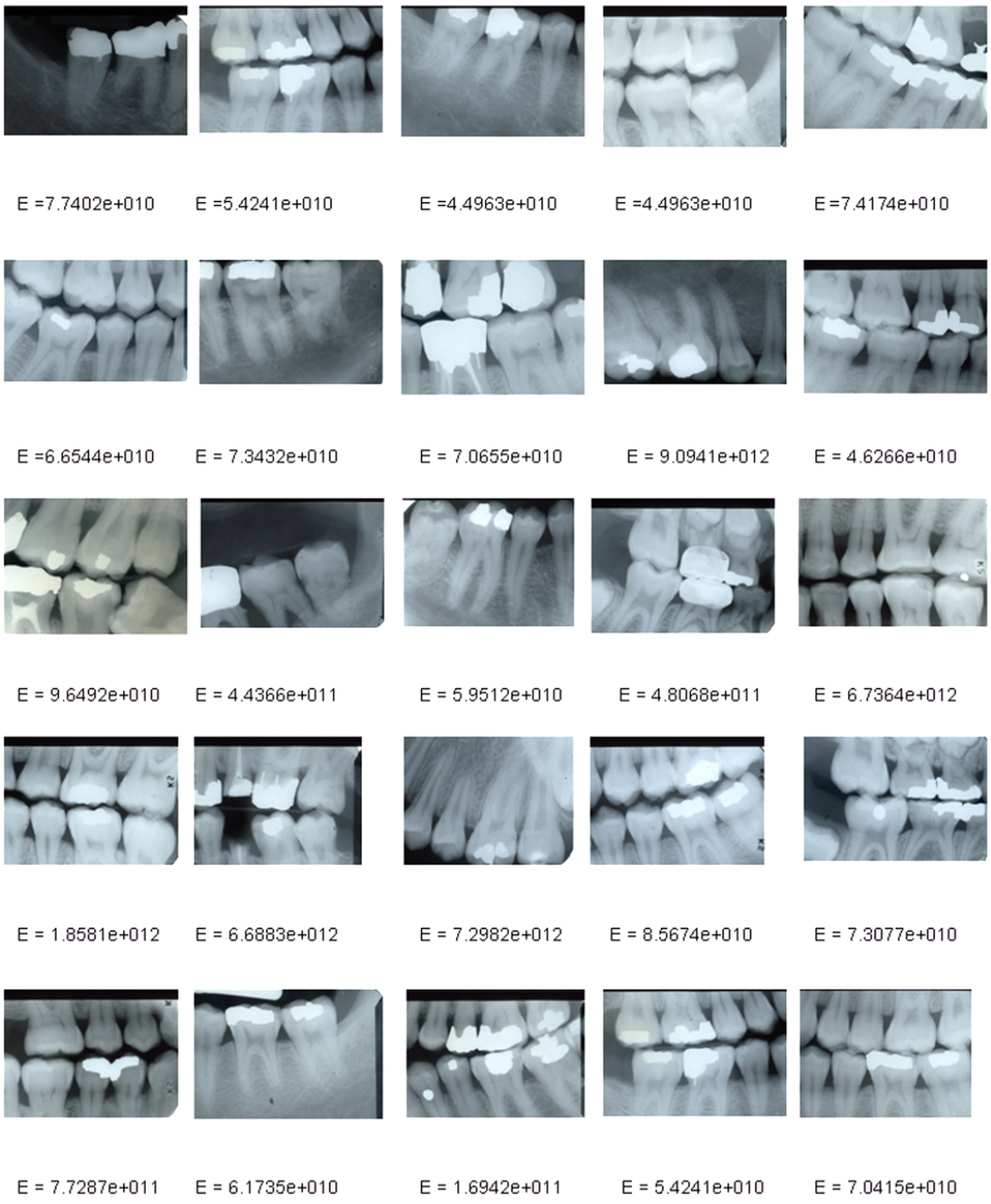

Figure 4.4: Results of a small identification trial on a database consisting of 25 x-rays

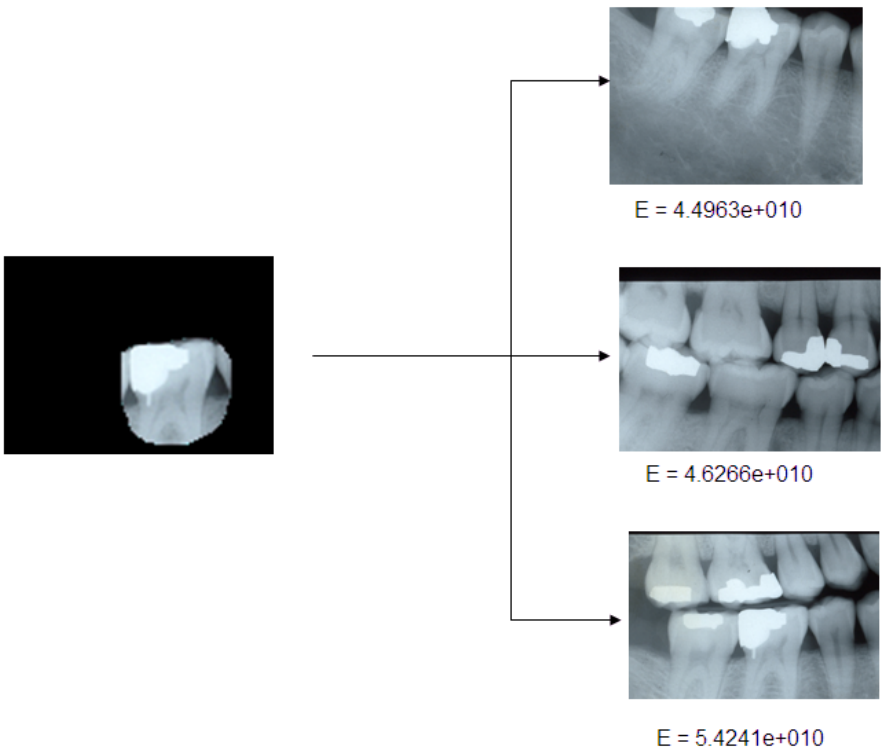

Figure 4.5: Top three matches

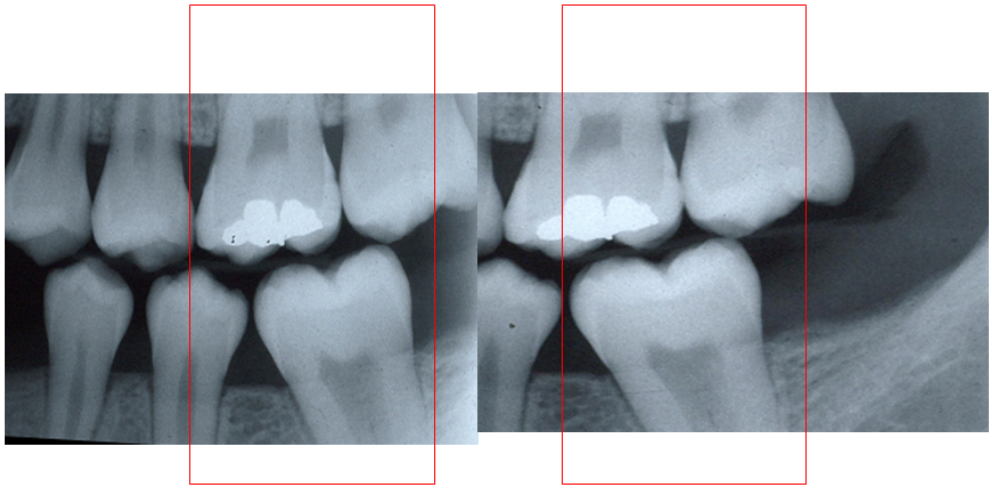

Figure 4.6: Two sample images with the area of overlap outlined

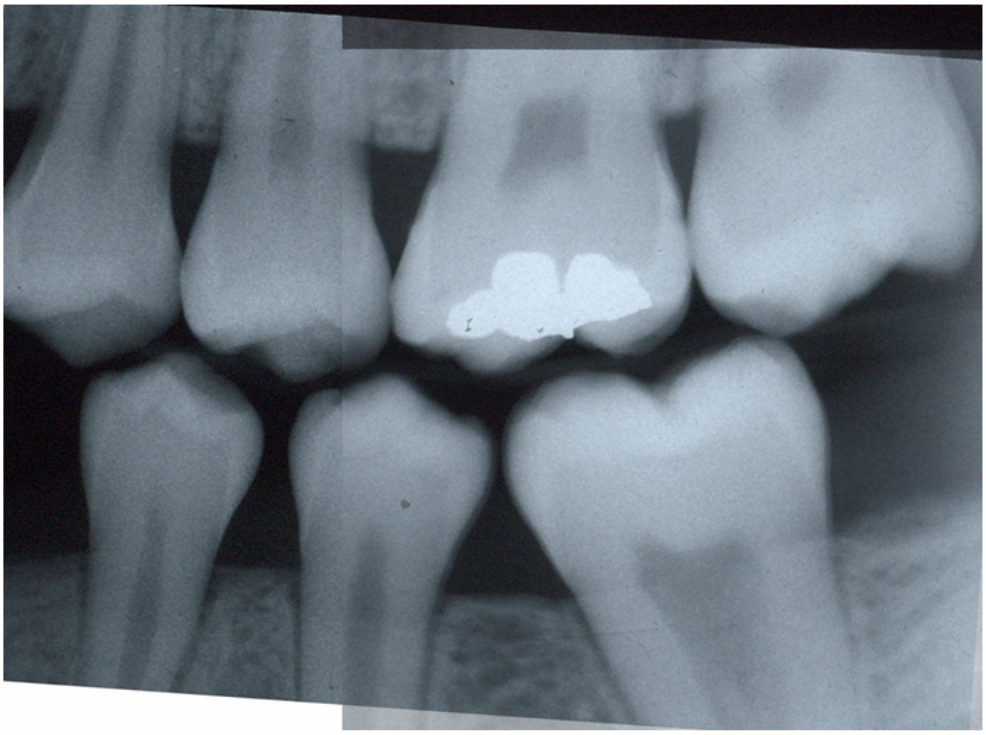

Figure 4.7: Registration of the two images

Figure 4.8: Difference image for the properly aligned x-rays

Chapter 5

Results

5.1 Single ROI and images approx. 225×190

Matching was performed over a single ROI, encompassing a single tooth with a part of its surrounding. All 150 of the PM/ROI pairs were used, constituting 150 identification scenarios. In 93 out of 150 cases (62% of trials), the correct match was in the top 1%. The correct match occurred in the top 10% and top 15% in 90% and 97% of the trials, respectively. Table 5.1 summarizes the test results. The count identifies the total number of cases for which the correct match was located in a given top %.

	1 %	2%	3 %	4 %	5%	10%	15%
count	93	100	106	112	117	134	145
% of trials	62	67	71	75	78	90	97

Table 5.1: Breakdown of the ranking of the top true match for images approx. 225×190 with a single ROI

In 56 out of the 150 cases, the correct match was the top-ranked match. In a real-life scenario, this means that 37% of the time the *first* radiograph the forensic odontologist looks at will be the *only* radiograph he/she needs to consider to establish the identity of the individual. The correct match was in the top ten in 64%

of the identification test cases. Table 5.2 shows the distribution of the top correct matches over all 150 trials.

rank	1	2	3	4	5	6	7	8	9	10
count	56	8	11	6	3	4	3	2	0	2

Table 5.2: The number of identification cases that ranked the correct match in the top ten for images approx. 225×190

Our methods performance in registering 150 PM/ROI images to correct AM images is displayed in Fig. 5.1 as a histogram of the top % true match ranking for images approx. sized at 225×190.

5.2 Single ROI and images approx. 550×380

Again, matching was performed over a single ROI, encompassing a single tooth with a part of its surrounding. All 150 of the PM/ROI pairs were used, accounting for a total 150 identification scenarios. The obtained results were almost identical to the ones obtained for the smaller images. In 93 out of 150 cases, the correct match was in the top 1% (again, 62% of the trials). The correct match occurred in the top 10% and top 15% in 90% and 97% of the tests respectively. Similarly to above, Table 5.3 summarizes all these test results.

	1 %	2%	3 %	4 %	5%	10%	15%
count	93	101	106	113	117	134	145
% of trials	62	67	71	75	78	90	97

Table 5.3: Breakdown of the ranking of the top true match for images approx. 550×380 with a single ROI

In 55 of 150 identification cases, or 36% of the trials, the correct match was the top-ranked match. The correct match was ranked in the top ten 64% of the time. Table 5.4 shows the distribution of the top correct matches over all 150 trials.

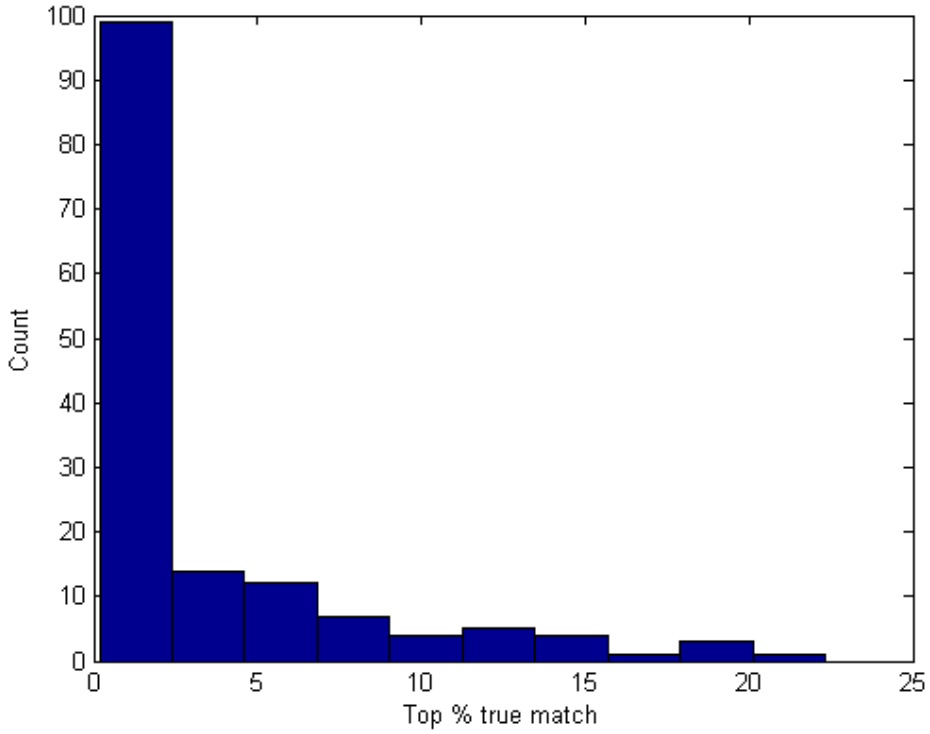

Figure 5.1: Histogram of the top % true match ranking for images approx. 225×190

rank	1	2	3	4	5	6	7	8	9	10
count	55	9	10	6	5	1	5	2	2	0

Table 5.4: The number of identification cases that ranked the correct match in the top ten for images approx. 550×380

Our methods performance in registering 150 PM/ROI images to correct AM images is displayed in Fig. 5.2 as a histogram of the top % true match ranking for images approx. sized at 550×380.

5.3 Comparison to mutual information

Using mutual information, a subset of 30 PM/ROI pairs is matched to the AM database consisting of 571 radiographs. We use FLIRT's implementation of mutual information [41] with 64 bins and tri-linear interpolation. A custom schedule file was created that was geared towards small angles ($< 10°$). This improved mutual information's chances of finding the globally optimal registration.

Mutual information returned the correct match as the top-ranked match 10 out of 30 identification trials (33% of the time), compared to our method's 18 out of 30 times (60% of the time). In 21 out of 30 cases (70% of the time), our method ranked the correct match in the top 1%. Mutual information ranked the correct match in the top 1% in 15 out of 30 cases (50% of the time). Direct comparison between the two methods is displayed in Figure 5.3 as a histogram showing the ranking of the correct match.

Mutual information does a good job at determining the correct match. However, the results show that the SSD method described here outperforms mutual information in the given problem domain. Figure 5.3 suggests that the SSD cost function is a more appropriate choice of an error metric for matching of dental x-rays.

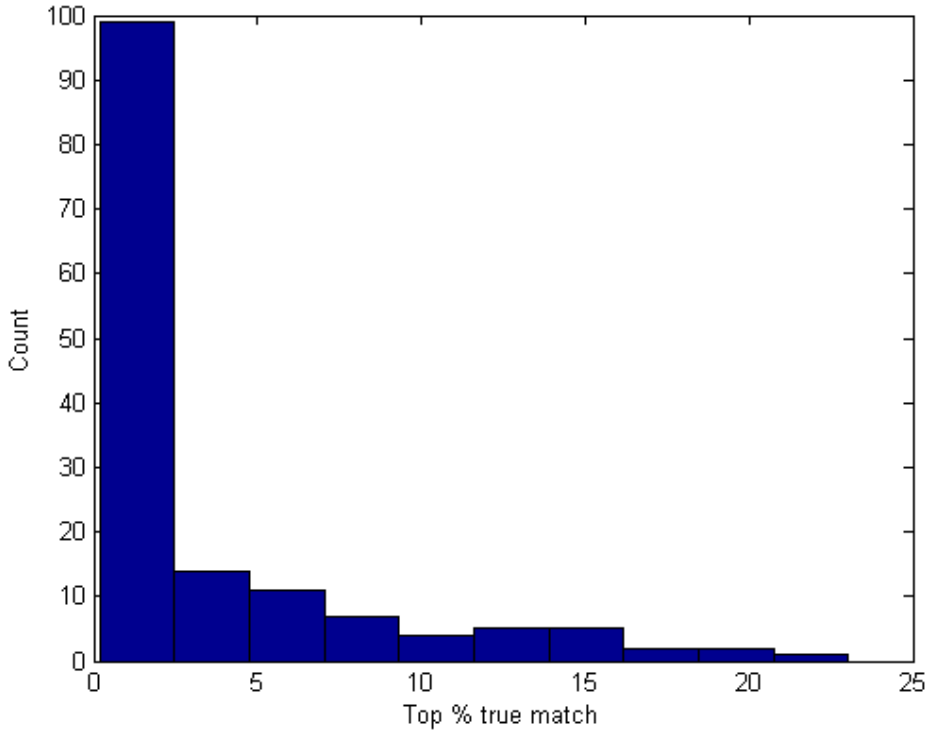

Figure 5.2: Histogram of the top % true match ranking for images approx. 550×380

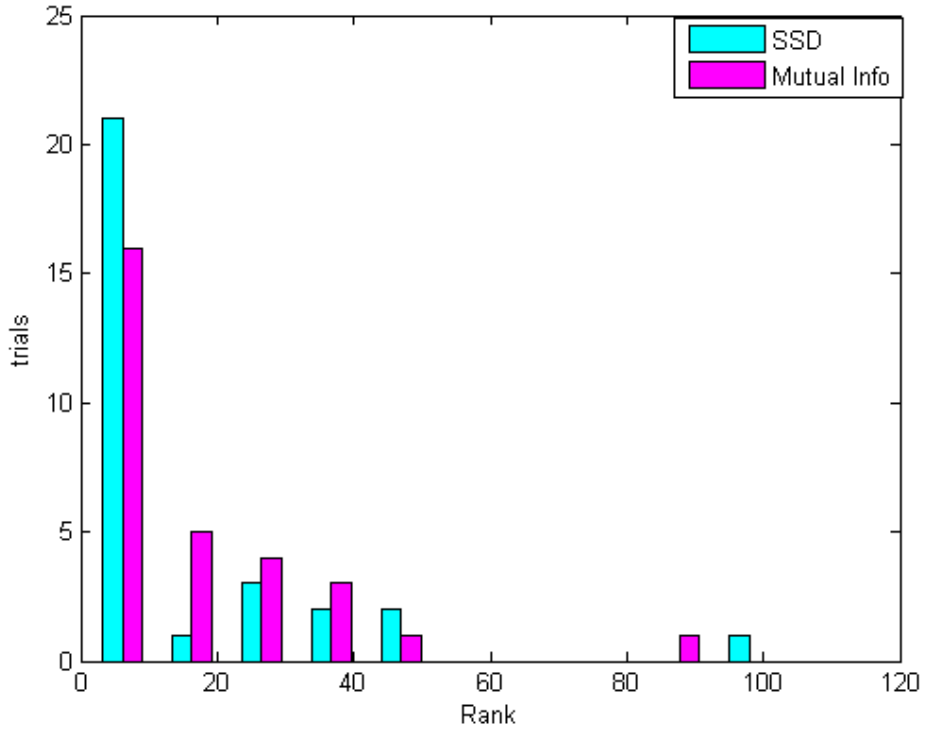

Figure 5.3: Histogram of the ranking for both the SSD and mutual information

Chapter 6

Conclusions and Future Work

6.1 Conclusions

The thesis proposed a computer-aided framework for efficient matching of dental radiographs for human identification purposes. Given a postmortem radiograph with a marked ROI, we search the database of antemortem radiographs in order to retrieve a closest match with respect to the ROI. The Weighted Sum of Squared Differences (SSD) cost function is used to express the degree of similarity between the two images. Unlike other iterative Least Squares methods that use local information for gradient descent, our method finds the globally optimal translation. The SSD cost function is slightly modified to account for the possibility of radiographs being acquired at different angles, as well as teeth shifting and rotating over time. The operation of rotation is linearly approximated. As mentioned, our method is global in terms of determining an optimal translation, but it is local in terms of determining an optimal angle.

The method was tested on a database consisting of 571 images. A total of 150 PM/ROI pairs were defined as identification scenarios. The ROI/PM pairs were matched to the database consisting of images sized at 225×190 and 550×380, resulting in 300 identification trials. For each identification trial, all possible shifts and linear intensity remappings are checked and recorded along with the associated

error (cost). The radiographs are ranked according to the error, with the smallest error indicating the best (top) match. For 37% of the trials, the correct match was the top-ranked match. In 64% of the trials, the correct match was ranked in the top ten. For 97% of the identification cases, the top match was located in the top 15%. The results depicted in Fig. 5.1 and Fig. 5.3 indicate that the increase in size of dental radiographs does not produce significant change in the effectiveness of our method. Other than some minor differences, the results are practically the same for both the images approximately sized at 550×380, and the images approximately half that size. Thus, reducing the size of radiographs, and consequently reducing the storage requirements needed to maintain the database, can be done without sacrificing the effectiveness of the matching method. The database storage requirements might not be of such importance in disaster situations where the number of unidentified individuals is relatively small, but they are, however, an important factor to consider in mass disaster situations and while maintaining Missing and Unidentified Person (MUP) databases. The MUP database can contain more than 100,000 people. If each person in the database had on average 15 dental radiographs approx. 150KB in size, then it would take $\approx$ 215GB to store the images alone. For radiographs approx. 40KB in size, the storage requirement drops down to 57GB.

Our experiments show that matching dental records using SSD is a viable method for human identification purposes. Note, however, that accurate dental forensic identification can only be made by a forensic odontologist through a point-by-point comparison of a complete set of mouth x-rays. The work shown here is intended to aid the forensic odontologists in the process possible match identification, while the positive dental identification still needs to be done by a forensic dental specialist.

6.2 Future Work

The matching within the scope of this thesis was done over a single tooth (in a single ROI). One possible avenue for future work involves using two or more ROI's in the matching process. One option is to do matching over a single ROI encompassing two

or more teeth. Another option involves using two separate ROI's in the process of matching and then combining the results. We anticipate that using multiple ROI's would give us even more accurate results. The PM/ROI image is matched to every image in the database regardless of to whom the image belongs. Thus, it is possible to have he top three ranked radiographs belonging to, e.g. patient 25, followed by the correct match ranked at 4. In reality, the correct match would be considered as a $2nd$ rank since the forensic odontologist would look at the radiographs belonging to patient 25 only once, despite the fact they are ranked 1, 2 and 3. Filtering of results (removing multiple occurrences of the same patient) is definitely a possible future work direction.

Storing metadata along with dental images will most likely result in improved matching capabilities of our method. Metadata would enable filtering capabilities prior to the actual matching process, consequently reducing the running time of the identification. Filtering of the data (e.g. based on the individual's sex) would reduce the size of the search domain, and with it, reduce the chances of a incorrect match getting a higher score than the true match.

Increasing the size of the database is the logical next step in this research. To truly test the effectiveness of this method, more radiographs need to be considered in matching. As shown by the current research in this field [5, 8],[16]-[24], the increase in the size of the database tends to hinder the effectiveness and the searching capabilities of the matching methods employed. The effects that an increase in the size of the database would have on our method still need to be investigated in more depth.

Incorporating rotation and translation with higher order intensity remappings is another direction for future work. We believe that the estimated rotation and translation parameters obtained with the higher order intensity remapping would result in an even higher percent of success. Furthermore, spatial scaling is not part of the transformation we are currently considering. Incorporating scaling into the SSD cost function is a next possible step in this research.

Bibliography

[1] R. DeLucia and T. Doyle, *Career planning in criminal justice, 3rd Edition.* Anderson Publishing Co., 1998.

[2] J. Wayman, A. Jain, D. Maltoni, and D. Maio, Eds., *Biometric Systems: Technology, Design and Performance Evaluation.* Springer, 2005, vol. 14.

[3] R. Bolle and S. Pankanti, *Biometrics, Personal Identification in Networked Society: Personal Identification in Networked Society.* Kluwer Academic Publishers, 1998.

[4] P. Stimson and C. Mertz, *Forensic Dentistry.* CRC Press, 1997.

[5] A. K. Jain, H. Chen, and S. Minut, *Audio- andVideo-Based Biometric Person Authentication*, ser. Lecture Notes in Computer Science. Springer Berlin and Heidelberg, August 2003, vol. 2688, ch. Dental Biometrics: Human Identification Using Dental Radiographs, pp. 429–437.

[6] D. Page, "Digital radiography gives forensic odontology more bite," *Forensic Magazine*, April 2005. [ONLINE] Available from: http://www.forensicmag.com/articles.asp?pid=38

[7] United States of America, Justice Department, "NCIC missing person and unidentified person statistics for 2005."[ONLINE] Available from: http://www.www.fbi.gov/hq/cjisd/missingpersons.htm

[8] D. E. M. Nassar and H. H. Ammar, "A prototype automated dental identification system (ADIS)," in *Proceedings of the 2003 Annual National Conference*

on Digital Government Research, ser. ACM International Conference Proceeding Series, vol. 130, 2003, pp. 1–4.

[9] American Board of Forensic Odontology, Inc., "Body identification guidelines," *Journal of American Dental Association*, vol. 125, no. 9, pp. 1244–1250, September 1994.

[10] I. A. Pretty and D. Sweet, "A look at forensic dentistry–part 1: The role of teeth in the determination of human identity," *British Dental Journal*, vol. 190, no. 7, pp. 359–366, April 2001.

[11] L. Kamb, "Part9: Flawed national dental database leaves dead nameless," February 26th, 2003. [ONLINE] Available from: http://seattlepi.nwsource.com

[12] Western Identification Network, Inc. [ONLINE] Available from: http://www.winid.org

[13] American Dental Association, "Forensic dentist's software speeds identification."October 28th, 2005. [ONLINE] Available from: http://www.ada.org

[14] American Society of Forensic Odontology, "Forensic odontology news," 1997.

[15] The Canadian Dental Association, "Communique," May 1997.

[16] G. Fahmy, D. Nassar, E. Haj-Said, H. Chen, O. Nomir, J. Zhou, R. Howell, H. H. Ammar, M. Abdel-Mottaleb, and A. K. Jain, *Biometric Authentication*, ser. Lecture Notes in Computer Science. Springer Berlin and Heidelberg, July 2004, vol. 3072, ch. Towards an Automated Dental Identification System (ADIS), pp. 789–796.

[17] A. Jain and H. Chen, "Matching of dental x-ray images for human identification," *Pattern Recognition*, vol. 37, pp. 1519–1532, 2004.

[18] H. Chen and A. Jain, "Dental biometrics: Alignment and matching of dental radiographs," *IEEE Transactions on Pattern Analysis and Machine Intelligence*, vol. 27, no. 8, pp. 1319–1326, August 2005.

[19] G. Fahmy, D. Eldin, M. Nassar, E. Jai-Said, H. Chen, O. Nomir, J. Zhou, R. Howell, H. H. Ammar, M. Abdel-Mottaleb, and A. Jain, "A web based tool for an automated dental identification system (ADIS)," in *Proceedings of the 2004 annual national conference on Digital government research*, ser. ACM International Conference Proceeding Series, 2004, pp. 1–2.

[20] A. Jain, J. Zhou, and M. Abdel-Mottaleb, "A content-based system for human identification based on bitewing dental x-ray images," *Pattern Recognition*, vol. 38, no. 11, pp. 2132–2142, 2005.

[21] J. Zhou and M. Abdel-Mottaleb, "Automatic human identification based on dental x-ray images," in *Biometric Technology for Human Identification*, ser. Proceedings of SPIE, vol. 38, no. 4, August 2004, pp. 373–380.

[22] M. H. Mahoor and M. Abdel-Mottaleb, "Classification and numbering of teeth in dental bitewing images," *Pattern Recognition*, vol. 38, no. 4, pp. 577–586, 2005.

[23] H. Chen and A. Jain, "Tooth contour extraction for matching dental radiographs," in *International Conference on Pattern Recognition*, ser. Proceedings of Pattern Recognition, vol. 3, August 2004, pp. 522–525.

[24] A. K. Jain and H. Chen, "Registration of dental atlas to radiographs for human identification," in *Proceedings of SPIE*, vol. 5779, March 2005, pp. 292–298.

[25] R. P. Woods, *Within-modality registration using intensity-based cost functions*. Orlando, FL, USA: Academic Press, Inc., 2000.

[26] A. Collignon, F. Maes, D. Delaere, D. Vandermeulen, P. Suetens, and G. Marchal, "Automated multi-modality image registration based on information theory," in *Information Processing in Medical Imaging*, vol. 14, Jund 1995, pp. 263–274.

[27] W. M. Wells III, P. Viola, H. Atsumi, S. Nakajima, and R. Kikinis, "Multi-modal volume registration by maximization of mutual information," *Medical Image Analysis*, vol. 1, no. 1, pp. 35–51, March 1996.

[28] M. Jenkinson and S. Smith, "A global optimisation method for robust affine registration of brain images," *Medical Image Analysis*, vol. 5, no. 2, pp. 143–156, June 2001.

[29] C. Studholme, D. L. G. Hill, and D. L. Hawkes, "An overlap invariant entropy measure of 3d medical image alignent," *Pattern Recognition*, vol. 32, pp. 71–86, 1999.

[30] J. P. W. Pluim, A. Maintz, and M. A. Viergever, "Mutual information-based registration of medical images: A survey," *IEEE Trans. Med. Imag.*, vol. 22, no. 8, pp. 986–1004, 2003.

[31] M. Omanovic and J. Orchard, "Efficient multimodal registration using least-squares," *Proc. Image Processing and Computer Vision (IPCV06)*, 2006.

[32] J. Orchard, "Efficient multimodal registration with a globally exhaustive alignment search," *IEEE Transactions on Image Processing*, (submitted) 2006.

[33] E. De Castro and C. Morandi, "Registration of translated and rotated images using finite fourier transforms," *IEEE Trans. Pattern Anal. Mach. Intell.*, vol. 9, no. 5, pp. 700–703, 1987.

[34] C. D. Kuglin and D. C. Hines, "The phase correlation image alignment method," in *Proc. Int. Conf. Cybernetics and Society*, 1975, pp. 163–165.

[35] G. Wolberg and S. Zokai, "Robust image registration using log-polar transform," in *Proc. Int. Conf. on Image Processing*, vol. 1, 2000, pp. 493–496.

[36] P. Pinnamaneni, S. Saladi, and J. Meyer, "Remote transformation and local 3d reconstruction and visualization of biomedical data sets in java3d," *Proceedings of SPIE*, vol. 4665, pp. 44–54, March 2003.

[37] A. J. Fitch, A. Kadyrov, W. J. Christmas, and J. Kittler, "Fast robust correlation," *IEEE Transactions on Image Processing*, vol. 14, no. 8, pp. 1063–1073, August 2005.

[38] J. Orchard, "Efficient global weighted least-squares translation registration in the frequency domain," in *International Conference on Image Analysis and Recognition*, ser. Lecture Notes in Computer Science, vol. 3565, 2005, pp. 116–124.

[39] J. W. Cooley and J. W. Tukey, "An algorithm for the machine calculation of complex fourier series," *Mathematics of Computation*, vol. 19, no. 90, pp. 297–301, April 1965.

[40] E. O. Bright, *The Fast Fourier Transform.* Prentice-Hall, Inc., 1974.

[41] M. Jenkinson and S. Smith, "A global optimisation method for robust affine registration of brain images," *Medical Image Analysis*, vol. 5, no. 2, p. 143156, 2001.